Journal of Colloid and Interface Science **248,** 443–454 (2002)
doi:10.1006/jcis.2001.8159, available online at http://www.idealibrary.com on IDEAL®

Simulation Studies of Phase Inversion in Agitated Vessels Using a Monte Carlo Technique

Leslie Y. Yeo, Omar K. Matar,[1] E. Susana Perez de Ortiz, and Geoffrey F. Hewitt

Department of Chemical Engineering and Chemical Technology, Imperial College of Science, Technology and Medicine, Prince Consort Road, London SW7 2BY, United Kingdom

Received May 25, 2001; accepted December 10, 2001; published online February 15, 2002

A speculative study on the conditions under which phase inversion occurs in agitated liquid–liquid dispersions is conducted using a Monte Carlo technique. The simulation is based on a stochastic model, which accounts for fundamental physical processes such as drop deformation, breakup, and coalescence, and utilizes the minimization of interfacial energy as a criterion for phase inversion. Profiles of the interfacial energy indicate that a steady-state equilibrium is reached after a sufficiently large number of random moves and that predictions are insensitive to initial drop conditions. The calculated phase inversion holdup is observed to increase with increasing density and viscosity ratio, and to decrease with increasing agitation speed for a fixed viscosity ratio. It is also observed that, for a fixed viscosity ratio, the phase inversion holdup remains constant for large enough agitation speeds. The proposed model is therefore capable of achieving reasonable qualitative agreement with general experimental trends and of reproducing key features observed experimentally. The results of this investigation indicate that this simple stochastic method could be the basis upon which more advanced models for predicting phase inversion behavior can be developed.

Key Words: **liquid–liquid dispersions; phase inversion; drop coalescence and breakup; Monte Carlo technique; stirred tanks; mixing.**

1. INTRODUCTION

The phenomenon whereby the phases of an agitated dispersion of two immiscible liquids interchange such that the dispersed phase spontaneously inverts to become the continuous phase and vice versa under conditions determined by the system's physical and physicochemical properties, phase volume ratio, and energy input is known as phase inversion. The prediction of the critical dispersed phase holdup, which is the point at which phase inversion occurs, has been a common pursuit since the infancy of research into phase inversion. The amount of experimentation required in order to predict the inversion point for a particular system would substantially decrease if a theoretically based correlation relating the phase inversion point to system parameters were available. Despite extensive research efforts, there have been relatively few attempts to predict the phase inversion point theoretically. Instead, various empirical correlations have been proposed but, unfortunately, there has been a considerable amount of variation between the predictions of these correlations and a satisfactory model has not been presented to date (1).

While there have been many computational models for describing a wide range of dynamic multiphase problems involving complex interfacial phenomena developed, few attempts to develop such models to predict the dispersed phase holdup at the inversion point have been made. Examples of stochastic models utilizing Monte Carlo techniques within this context include the work of Jiang *et al.* (2) on the rheological behavior of foams, as well as that of Hsia and Tavlarides (3), Ribeiro *et al.* (4), and Balmelli and Steiner (5) to model the dynamic behavior of dispersions in agitated vessels.

A stochastic model attempting to simulate phase inversion in a dispersion of spherical drops existing in a thin annular liquid film flowing around a tube wall via a Monte Carlo technique has been developed by Juswandi (6). This model is limited by the fact that it does not accurately reflect the actual mechanisms behind the inversion process. The model does not take into account the hydrodynamics of the coalescence process; film drainage times and contact times have not been incorporated into the coalescence model. While Juswandi (6) indicates that his results are in good agreement with the experimental results of Brooks and Richmond (7), this has not been shown in great detail; no attempts were made to match the experimental geometry and flow conditions.

In our work, the model of Juswandi (6) is modified for liquid–liquid dispersions occurring in agitated vessels. The dynamics of phase inversion is modeled using a Monte Carlo-type scheme for drop coalescence and breakup together with the criterion of interfacial energy minimization at the inversion point. Attempts are made to overcome the limitations found in the model by accounting for the hydrodynamics of drop coalescence. In addition, the model also includes a framework for dealing with the interpenetration of drops, a feature that becomes extremely prominent at high-phase volume holdups in models wherein no account is taken of drop deformation. Using this scheme, predictions of phase inversion are obtained for a variety of system parameters.

[1] To whom correspondence should be addressed.

0021-9797/02 $35.00

Given the spontaneity of the inversion process, Luhning and Sawistowski (8) have suggested that the total energy content of the system is minimized at the point of phase inversion. However, since it has been found that there is always a reduction in the interfacial energy at the phase inversion point and since no measurable change in the power input was observed (9), the minimization of the total energy which forms the criterion for phase inversion must come from a redistribution between the interfacial energy and the total kinetic energy of the system. Fakhr-Din (9) noted that the interfacial energy changes were of magnitudes comparable to the total system energy and hence concluded that the change in kinetic energy would be small compared to the change in the interfacial energy upon inversion. Therefore, the modeling of phase inversion by minimizing the interfacial energy satisfies the criterion of total system energy minimization. This criterion for the determination of the phase inversion point, i.e., the minimization of the interfacial energy, also used in the work of Tidhar *et al*. (10), is thus used in this model. It should be noted that this criterion does not bring to bear any light on the mechanism by which phase inversion occurs, and therefore we do not make any claims that this model suggests such. While careful attempts have been made to simulate the inversion process as accurately as possible using the physics of drop interactions, we do recognize that there still remain limitations associated with this stochastic method. This model therefore is not intended to provide further understanding of the mechanisms for the phase inversion phenomenon. At best, this model is a speculative tool for evaluating the ability of such stochastic methods in predicting conditions under which complex phenomena such as phase inversion occurs. It is our hope that the results presented here will encourage this simple model to serve as a basis for the development of more advanced models.

The remainder of this paper is organized as follows. A description of the model is provided in Sections 2 and 3, while Section 4 is devoted to a discussion of model predictions. Finally, concluding remarks are provided in Section 5.

2. GENERAL APPROACH

The modified model retains some features of the algorithm for the Monte Carlo technique employed by Juswandi (6). The following assumptions are made:

- The drops are initially spherical.
- The initial dispersion drop size distribution is uniform. Each drop has a size corresponding to the Sauter mean (i.e., the surface area to volume weighted average) diameter, d_{32} (m).
- All drops are initially placed in a lattice in a face-centred cubic configuration, the dimensions of the lattice determined by the dispersed phase holdup and the initial drop size.

The main steps of the algorithm, shown in Fig. 1, are:

1. A randomly chosen drop is translated as described below.
2. The possibility of the moved drop coalescing with a neighboring drop is considered: In the event of coalescence, the resulting coalesced drop is placed in the original position of the neighboring drop with which the drop chosen in step 1 coalesced. Should the size of the resulting coalesced drop exceed the maximum stable drop size, $d_{\max}$ (m), the drop subsequently breaks up again into a drop with size $d_{\max}$ and a smaller drop.
3. Another random drop is chosen and the probability that it breaks up is checked (together with the possibility of the daughter drops recoalescing with other neighboring drops); in the event that breakup occurs, one daughter drop is placed at the original location of the mother drop whereas the other daughter drop is placed randomly in the dispersion lattice.

The random translation of the drops within the dispersion lattice, step 1, is modeled using a method somewhat similar to the Metropolis Monte Carlo method (11):

$$x \rightarrow x + \alpha(2\xi_1 - 1), \quad [1]$$

$$y \rightarrow y + \alpha(2\xi_2 - 1), \quad [2]$$

$$z \rightarrow z + \alpha(2\xi_3 - 1). \quad [3]$$

This is illustrated in Fig. 2. In Eqs. [1] to [3], x, y, and z are the coordinates of the drops, α is an adjustable parameter governing the magnitude of the displacement and ξ_i ($i = 1, 2, 3$) are random numbers between 0 and 1. By varying α between 5 and 50% in the simulations, it can be concluded that the results are largely insensitive to α, and thus a value of 10% of the maximum lattice diameter was used.

3. MODEL DEVELOPMENT

In this section, the development of the model to predict the phase inversion point in agitated vessels is presented. The fundamental hydrodynamic processes and the analytical expressions describing the corresponding probabilities that describe these processes are summarized in Table 1.

3.1. Breakup Probability

In (6), the possibility of drop breakup is considered by comparing the breakup probability to a random number that is generated. We model this breakup probability, Ω, by taking into account the probability of breakup due to the effect of inertia on the drop and the probability of breakup to account for viscosity effects:

$$\Omega = \Phi\left[\exp\left(-\frac{\eta_d}{\eta_c}\right)\right] + (1 - \Phi)\left[\exp\left(\frac{\mathrm{We}}{\mathrm{We}_{\mathrm{crit}}} - 1\right)\right]. \quad [4]$$

η_c and η_d are the continuous and the dispersed phase viscosities (Pa · s), respectively, and Φ is a weighting factor that will be defined later in this section. We is the Weber number, defined by (12)

$$\mathrm{We} = \frac{\rho\overline{u^2}d}{\sigma}. \quad [5]$$

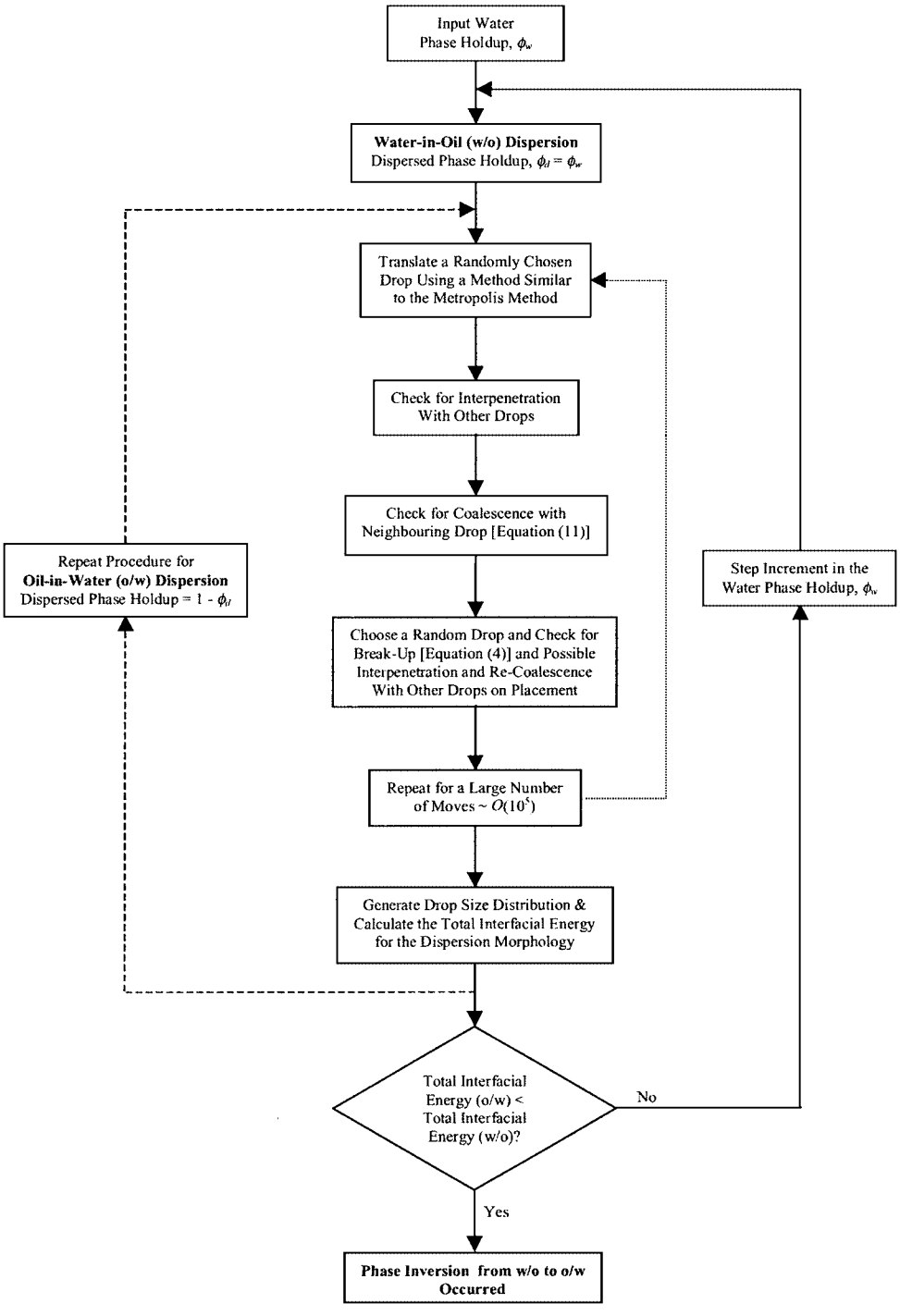

FIG. 1. Algorithm for the phase inversion model.

Here, ρ denotes the density (kg/m^3), σ the interfacial tension (N/m), and d the drop diameter (m); $\overline{u^2}$ is the mean square of the relative velocity fluctuations between two diametrically opposite points on the surface of a drop (m^2/s^2) (13):

$$\overline{u^2} \sim (\varepsilon d)^{\frac{2}{3}}. \qquad [6]$$

For a fully baffled turbine mixer at high Reynolds numbers, the turbulent energy dissipation per unit mass of fluid, ε (J/kg · s), assumes the relationship

$$\varepsilon \sim N^3 D_I^2, \qquad [7]$$

N being the agitation speed (s^{-1}) and D_I the impeller diameter

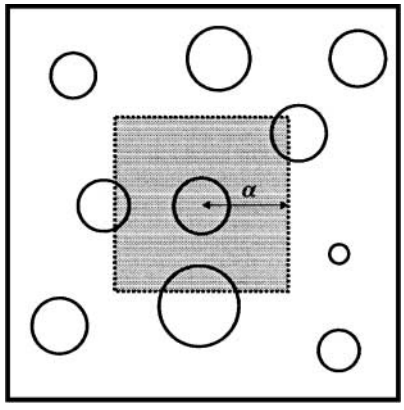

FIG. 2. The Metropolis Method illustrating the movement of a drop within the confines of the maximum allowed displacement, α.

(m). Similarly, a critical Weber number, We_{crit}, above which drop breakup occurs can be defined by replacing d in Eq. [5] with d_{max} (12):

$$We_{crit} = \frac{\rho \overline{u^2} d_{max}}{\sigma}. \quad [8]$$

The first term in Eq. [4] considers the effect of viscosity on breakup. In the turbulent breakup of drops in the inertial subrange, it was found that for large dispersed phase viscosities, the viscous stresses due to the internal flow within the drop dampens drop deformation (14). Therefore, the probability of breakup is low if the ratio of the dispersed phase viscosity to that of the continuous phase is large. The second term in Eq. [4], on the other hand, corresponds to the probability of breakup due to the effect of the inertial flow conditions on the drop; the larger the drop, the greater the probability of it breaking up. Since the Weber number used is a local one, pertaining to the selected drop for which the probability of breakup is being evaluated upon, this probability is related to the chance that this particular drop flows through a zone in the agitated vessel where the turbulent kinetic energy is sufficiently high to cause breakup. Thus, by incorporating this localized Weber number into the breakup probability, the inhomogeneity of turbulence, which is common in agitated vessels, is taken into account. In the event that the localized Weber number is equal to or exceeds its critical value, breakup is certain to occur, and the probability of breakup due to inertial effects is set to a value of unity.

Φ, the weighting factor between viscous and inertial breakup in Eq. [4], is given by the ratio of the size of the smallest eddies which dissipate energy due to viscous effects, as defined by the Kolmogoroff length scale (m), $\eta = (\nu^3/\varepsilon)^{\frac{1}{4}}$ where ν is the kinematic viscosity (m^2/s), to the diameter of the drop for which the probability of breakup is to be evaluated on. Thus,

$$\Phi = \frac{\eta}{d} \quad \text{for } \eta < d, \quad [9]$$

and

$$\Phi = 1 \quad \text{for } \eta \geq d. \quad [10]$$

If the drops are much larger than the Kolmogoroff length scale, the viscous stresses acting upon the drops are negligible in comparison with the turbulent pressure fluctuations (15, 16). Therefore, the drop is more likely to be broken up due to inertial effects rather than viscous effects. However, if the drop size is comparable to the Kolmogoroff length scale, then viscous shear plays an increasingly dominant role in the breakup process.

TABLE 1

Summary of the Fundamental Drop Hydrodynamic Processes and the Corresponding Analytical Expressions for the Probabilities Describing Them

Hydrodynamic process	Corresponding expression for the probability	Reference
1. Drop breakup	$\Omega = \Phi\left[\exp\left(-\frac{\eta_d}{\eta_c}\right)\right] + (1-\Phi)\left[\exp\left(\frac{We}{We_{crit}} - 1\right)\right]$	—
2. Drop coalescence	$\lambda_1 = \exp\left[-\frac{K_1 \eta_c \rho_c D_1^2 N^3}{\sigma^2}\left(\frac{v_1^{1/3} v_2^{1/3}}{v_1^{1/3}+v_2^{1/3}}\right)^4\right]$	(17)
	$\lambda_2 = \exp\left[-\frac{K_2 \sigma \left(v_1^{2/3}+v_2^{2/3}\right)(v_1+v_2)}{\rho_d N^2 D_1^{4/3} v_1 v_2 \left(v_1^{2/9}+v_2^{2/9}\right)}\right]$	(18)
	$\lambda(v_1, v_2) = \lambda_1(v_1, v_2) + \lambda_2(v_1, v_2) - \lambda_1(v_1, v_2)\lambda_2(v_1, v_2)$	(18)
3. Drop deformation	$\Psi = \exp\left(-\frac{E_d}{E_k}\right)$	—

3.2. *Coalescence Probability*

The rate of coalescence is dependent on both the probability that two colliding drops coalesce as well as the frequency at which these collisions occur. While the collision frequency is not explicitly evaluated in this stochastic model, it is inherent in the classical Monte Carlo move. The greater the phase holdup and hence the number density of the drops, the greater the likelihood that the selected drop will encounter and collide with another drop in the vicinity of its random move.

In order for coalescence to take place between two colliding drops, the intervening continuous phase film separating the two drops must drain to the critical film rupture thickness. In order for this to be achieved, the drops must remain in contact with each other for a period longer than the time it takes for the film to drain to the critical film thickness. The coalescence probability, λ, can thus be described generally by the following expression suggested by Coulaloglou and Tavlarides (17),

$$\lambda = \exp\left(-\frac{t_{drain}}{t_{contact}}\right), \quad [11]$$

where t_{drain} is the film drainage time (s) and $t_{contact}$ the time

during which colliding drops remain in contact with each other (s). The full expression for the coalescence probability between two deformable drops, λ_1, was given in (17) as

$$\lambda_1 = \exp\left[-\frac{K_1\eta_c\rho_c D_I^2 N^3}{\sigma^2}\left(\frac{v_1^{1/3}v_2^{1/3}}{v_1^{1/3}+v_2^{1/3}}\right)^4\right]. \quad [12]$$

K_1 is a dimensional constant (m^{-2}) related to the film thickness at coalescence, ρ_c the continuous phase density (kg/m^3), and v_1 and v_2 are the volumes of the coalescing drops (m^3).

Sovová (18), however, suggested that the coalescence probability of (17) given by Eq. [12] only allows for the preferential coalescence of small drops. The following expression was therefore proposed as an alternative to the coalescence probability of (17) in Eq. [12] based on an analysis of the impaction energy of the colliding drops,

$$\lambda_2 = \exp\left[-\frac{K_2\sigma\left(v_1^{2/3}+v_2^{2/3}\right)(v_1+v_2)}{\rho_d N^2 D_I^{4/3} v_1 v_2\left(v_1^{2/9}+v_2^{2/9}\right)}\right], \quad [13]$$

where K_2 is a dimensionless constant and ρ_d the dispersed phase density (kg/m^3). The numerator of the argument describes the term for the drop interfacial energy, whereas the denominator describes the energy due to the collision of the drops. Sovová (18) suggests that this expression allows for the preservation of small drops produced by the breakup process.

A combination of both mechanisms is used, given by the following expression for the overall coalescence probability, λ, which describes the joint probability between two events (18):

$$\lambda(v_1, v_2) = \lambda_1(v_1, v_2) + \lambda_2(v_1, v_2) - \lambda_1(v_1, v_2)\lambda_2(v_1, v_2). \quad [14]$$

By comparing the coalescence probability above with a random number generated, the coalescence (or noncoalescence) of the drop moved at random with another drop can be determined.

While the constant K_2 in Eq. [13] is obtained by directly fitting the parameter to experimental data, the constant K_1 can be further defined as

$$K_1 \sim \frac{1}{h_c^2} - \frac{1}{h^2}, \quad [15]$$

where h is the intervening film thickness at the initial contact of the drops (m) and h_c is the critical film rupture thickness (m). K_1 thus takes into account the time taken for film drainage as the drops deform. An expression for the critical film rupture thickness, h_c, determined by equating the van der Waals forces to the driving force behind film drainage is given by (19)

$$h_c \sim \left(\frac{AR_{eq}}{8\pi\sigma}\right)^{\frac{1}{3}}, \quad [16]$$

where A is the Hamaker constant (J) and R_{eq} the equivalent radius of the coalescing drop pair with radii r_1 and r_2 (m) defined as

$$\frac{1}{R_{eq}} = \frac{1}{2}\left(\frac{1}{r_1}+\frac{1}{r_2}\right). \quad [17]$$

3.3. Drop Size Correlations

The correlations for the maximum stable drop size, d_{max}, and for the Sauter mean diameter, d_{32}, that are readily available in literature are pertinent to "steady-state" conditions rather than to transient processes. However, since the criterion for the phase inversion employed requires a comparison of the total interfacial energies for both dispersion morphologies at steady state for a given phase holdup where the interfacial energies reach a steady equilibrium state, the use of these correlations to characterize the drop sizes is justified.

In the literature, the majority of correlations for the maximum stable drop diameter, d_{max}, assume the relationship

$$\frac{d_{max}}{D_I} = C_1 We_I^{-0.6}, \quad [18]$$

where C_1 is a constant and We_I is the impeller Weber number, defined by

$$We_I = \frac{\rho_c N^2 D_I^3}{\sigma}. \quad [19]$$

In this work, a value for C_1 of 9146.63 was used, which was obtained by regression of the experimental data found in (20).

To evaluate the Sauter mean diameter, d_{32}, the correlation of Chen and Middleman (21) was employed:

$$\frac{d_{32}}{D_I} = 0.045 We_I^{-0.57}. \quad [20]$$

It will be seen in Section 4.1 that model predictions are relatively insensitive to the choice of Sauter mean diameters used for the initial drop sizes. Therefore, the correlation of (21) given by Eq. [20] was used instead of more complicated forms for the Sauter mean diameter for the purposes of simplicity and because the empirical constant was readily available.

3.4. Interfacial Mobility and Film Drainage Time

The drainage time of the film to its critical thickness is dependent on the mobility of the interfaces, which is governed by the tangential stresses exerted on the film by the drops that arise from the internal circulation in the drops. Interfaces are said to be

immobile when the dispersed phase viscosity is high compared to that of the continuous phase or when surfactants are present to retard the drainage of the film by increasing the interfacial dilational and shear viscosities, or by introducing interfacial tension gradients which cause the Marangoni effect.

Fully mobile interfaces, which form the opposite limiting case, arise when the continuous phase viscosity is very large compared to that of the dispersed phase such that the tangential stresses exerted by the drops onto the film are negligible. Partially mobile interfaces are found in pure liquid–liquid dispersions, whereby the viscosity ratio of the dispersed and continuous phases are moderate. Abid and Chesters (22) suggest that the range of dispersed to continuous phase viscosity ratios for which partially mobile interfaces are valid is between 10^{-2} and 10^2, although this range becomes narrower for the coalescence of smaller drops. The upper limit is confirmed by the results of Bazhlekov *et al*. (23), who also suggest that interfaces are immobile for viscosity ratios greater than 10^4. Fully mobile interfaces are encountered typically in gas dispersed systems. The mobility of interfaces is therefore a strong function of the viscosity ratio and the presence of surfactants; either factor increasing interfacial mobility will speed up the film drainage, resulting in higher probabilities of coalescence.

For practical liquid–liquid dispersions in which surfactants are not present, the interface is partially mobile. For these cases, equations governing drainage times have been proposed by Chesters (19), Tsouris and Tavlarides (24), Li and Liu (25), and Liu and Li (26). It should be noted that the expression for coalescence probability by Coulaloglou and Tavlarides (17) in Eq. [12] is based on an analysis for film drainage of immobile interfaces. Nevertheless, due to the absence of detailed systematic studies on coalescence probabilities for partially mobile interfaces, we have opted to use the expression described by Eq. [12]. Coulaloglou and Tavlarides (17) have numerically taken into account the interfacial mobility of the film since they have fitted their dimensional constant to their experimental data for a water/kerosene–dichlorobenzene system in which no surfactants were present. This is confirmed by the drainage times obtained with this constant, which were found to be on the order of 1 s. This is comparable to drainage times for partially mobile interfaces as opposed to the drainage times obtained for the immobile case, which is on the order of 1000 s as seen in the results of Li and Liu (25).

3.5. Penalizing Translation Moves: Drop Interpenetration

At high-phase volume holdups, attempts to move drops represented as rigid spheres randomly within a fixed volume under a constraint of strict no interpenetration in a Monte Carlo-like scheme become increasingly difficult. This is perhaps not surprising since a packing efficiency of 60% has been found for optimized random loose packing of uniform rigid spheres (27). In reality, however, drops tend to deform, allowing for even greater packing fractions to be reached. Since phase inversion holdups well in excess of 60% are common, imposing a no interpenetration constraint is unfeasible; this constraint will be relaxed. The penetration of one drop into another will, however, be interpreted as "deformation" of the liquid drops in response to flow conditions and interactions with other drops within the complex flow field in an agitated vessel. This allows the model to be extended to high-phase volume holdups.

The translation of a randomly chosen drop may result in its interpenetration with a number of drops. Multiple-drop interpenetration within a simulation is treated by selecting a drop at random from a neighbor list of all drops, which have interpenetrated the translated drop. If the move fails, another interpenetrating drop is selected at random and the process is repeated. If the moves fail for all the interpenetrating drops, no moves are permitted for the chosen translated drop. This drop is then replaced and another selected at random for translation.

The extent of deformation will be determined by a probability, which governs the translation of a drop, step 1 in Section 2, and penalizes large degrees of interpenetration. This probability, denoted by Ψ, is given by (28),

$$\Psi = \exp\left(-\frac{E_d}{E_k}\right), \qquad [21]$$

where E_d is the energy required to deform a drop (J) and E_k is the total kinetic energy of the system (J), which is available to induce the deformation. E_d is given by

$$E_d = \sigma \Delta A_i, \qquad [22]$$

where ΔA_i is the increase in the interfacial area as a result of the deformation process (m^2). E_k can be expressed by

$$E_k \sim \rho_c \overline{u^2} d^3, \qquad [23]$$

where $\overline{u^2}$ is the characteristic difference of the velocity squared at different positions on the surface of the drop (m^2/s) given by Eq. [6]. Translation of the randomly chosen drop will be accepted provided Ψ is larger than a random number. It should be noted that Eqs. [21] to [23] give a form for the probability similar to that used by Lachaise *et al*. (29) for the probability of breakup in a turbulent flow field.

The drops are assumed to deform into prolate spheroids, as shown in Fig. 3, an assumption similar to that of Vaessen (30). The origins of the spheroids are assumed to be the centers of the originally undeformed spherical drops. The resulting film thickness between the spheroids, h (m), is obtained by equating the film drainage time, t_{drain} (s), for two deformable drops of diameters d_1 and d_2 (m) (17, 19),

$$t_{drain} = \frac{3\eta_c F}{16\pi\sigma^2}\left(\frac{1}{h_c^2} - \frac{1}{h^2}\right)\left(\frac{d_1 d_2}{d_1 + d_2}\right)^2, \qquad [24]$$

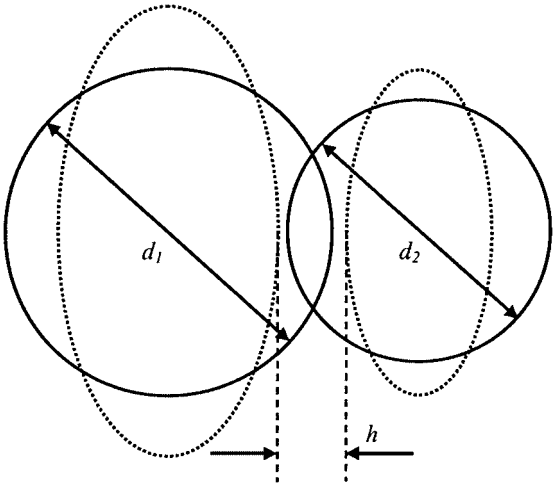

FIG. 3. Schematic representation of the deformation of two initially spherical drops of diameter d_1 and d_2 to prolate spheroids. The thickness of the thin continuous fluid film between the deformed drops is denoted by h.

in which h_c is given by Eq. [16], with that for rigid drops (17):

$$t_{\text{drain}} = \frac{\pi \eta_c}{F}\left(\frac{d_1 d_2}{d_1 + d_2}\right)^2. \qquad [25]$$

In Eqs. [24] and [25], F is the force compressing the two drops with diameters d_1 and d_2 in meters (N) (17):

$$F \sim \rho_c \overline{u^2}\left(\frac{d_1 d_2}{d_1 + d_2}\right)^2. \qquad [26]$$

Determination of h permits the calculation of the equatorial radii, a_1 and a_2 (see Appendix), while the other dimension of the spheroid, the polar radii c_1 and c_2, can then be obtained by volume conservation. Both dimensions of the prolate spheroids are restricted to the maximum stable drop size, $d_{\max}$. As shown in Fig. 4, Ψ decreases with increasing degrees of drop interpenetration for a fixed agitation speed, and increases with agitation speed for a fixed degree of interpenetration.

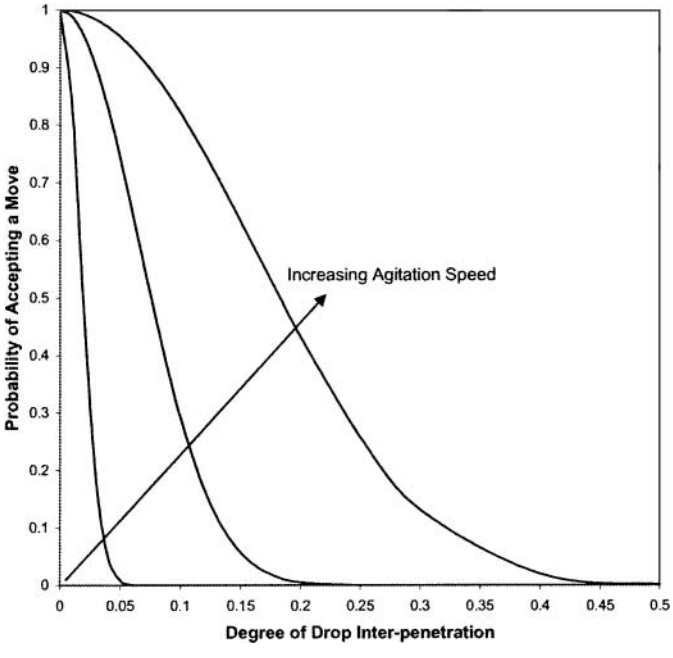

FIG. 4. Parametric dependence of the probability of accepting drop translation moves on agitation speed, as a function of the degree of drop interpenetration.

4. RESULTS AND DISCUSSION

We begin our discussion by assessing the sensitivity of our results to initial conditions.

4.1. Drop Initial Conditions

Figure 5 depicts the parametric dependence on chosen initial conditions of the total interfacial energy per volume against the number of translation moves. The sensitivity of the system to variations in the initial mean drop sizes, the initial number of drops, the polydispersity and the packing of the system was investigated. Inspection of Fig. 5 reveals that the final energy state of the system becomes largely independent of initial drop conditions for a sufficiently large number of moves; steady-state is reached after about approximately 200,000 moves. Since phase inversion holdups in this model are obtained mainly from a comparison of the interfacial energies of each dispersion morphology, it can be concluded that the phase inversion holdup itself is insensitive to the initial conditions.

Fluctuations about a mean value are observed if the initial mean drop diameter is small. This can be explained by the fact that for small initial mean drop sizes, the coalescence probability is close to unity, a consequence of the coalescence probability of (17) given in Eq. [12], which allows for the preferential coalescence of small drops. As a result, the total number of drops falls quickly and hence the total interfacial energy of the system is very sensitive to any perturbations in the coalescence and breakup probabilities. An inspection of Fig. 5 also reveals that the mean drop size at steady state generated by the model is in agreement with the correlation for the Sauter mean diameter of Chen and Middleman (21) used for the initial drop size, given by Eq. [20]. This demonstrates the ability of the model to predict the Sauter mean drop sizes given the prevailing physical and physicochemical conditions governing the dispersion.

4.2. Effect of the Viscosity Ratio on the Phase Inversion Holdup

The effect of the water-to-oil viscosity ratio, λ, on the phase inversion holdup from a water-in-oil dispersion to an oil-in-water dispersion in an equal density system at various agitation speeds

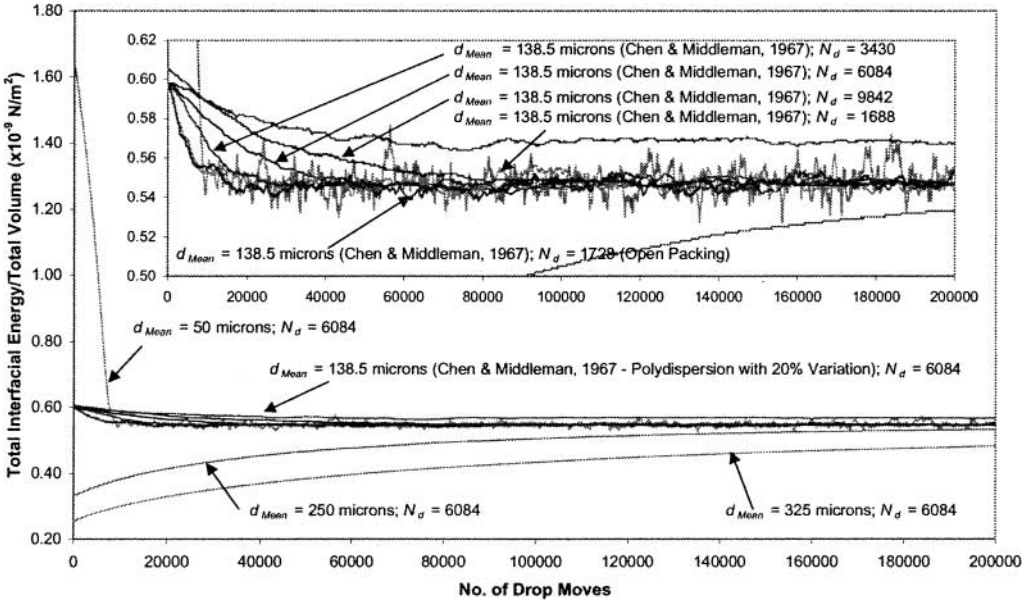

FIG. 5. Evolution of the total interfacial energy of the system with the number of random moves. (The inset shows a magnification of the curves; d_{mean} is the initial mean drop diameter and N_{d} is the initial number of drops.)

is illustrated in Fig. 6. The overall trend is that of an increase in the inversion holdup with increasing λ, as observed by Selker and Sleicher (31). Furthermore, the model predictions exhibit relatively good agreement with the experimental observations and the relation of Yeh *et al*. (32) given by

$$\frac{\phi_{\text{d,i}}}{1-\phi_{\text{d,i}}} = \sqrt{\frac{\eta_{\text{d}}}{\eta_{\text{c}}}}, \qquad [27]$$

which is also plotted in Fig. 6 where $\phi_{\text{d,i}}$ is the dispersed phase holdup at the inversion point. It should be noted, however, that the experiments of Yeh *et al*. (32) were performed by shaking a flask manually to produce the dispersion. The mixing intensity was thus uncontrollable and the dispersion morphology had to be determined by visual inspection. Although the present work involves the simulation of concentrated dispersions in an agitated vessel, the scaling relation of Arirachakaran *et al*. (33) for phase

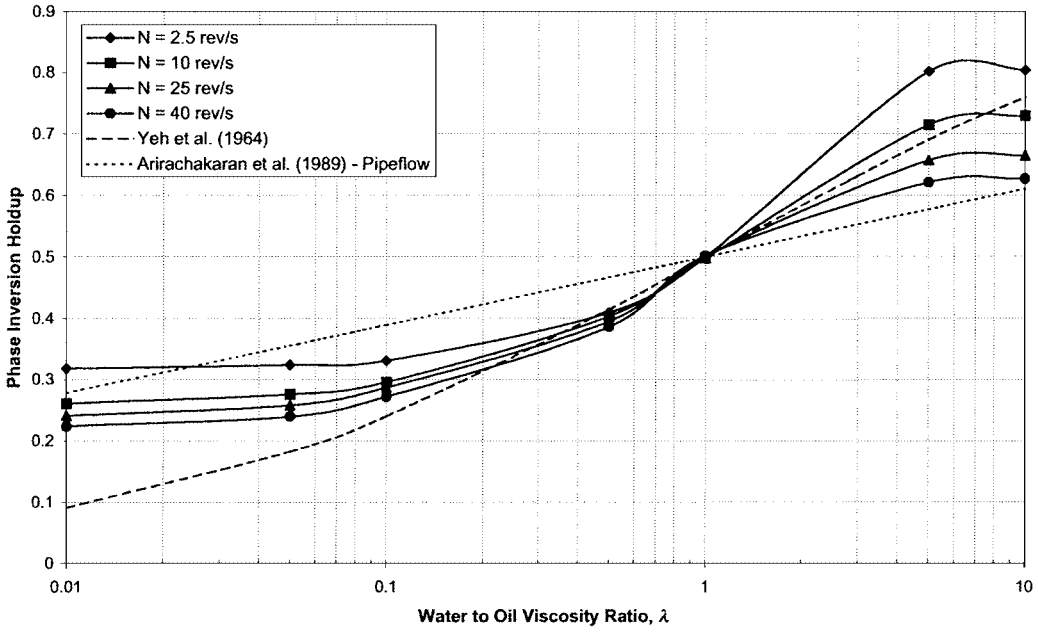

FIG. 6. Effect of water-to-oil viscosity ratio on inversion holdup for an equal density system. (Note that the lines were added to aid clear viewing of the trends rather than on a theoretical basis.)

inversion occurring in pipe flow is also shown in Fig. 6 for comparative purposes.

The general trend observed in Fig. 6 can be explained by examining the effect of λ, the water-to-oil viscosity ratio, on the relative rates of coalescence and breakup and the resultant shifts in the water-in-oil (w/o) and oil-in-water (o/w) energy curves. An increase in λ results in an increase and a decrease in the coalescence probability of w/o dispersions and o/w dispersions, respectively. This is due to the fact that the coalescence probability decreases with increasing continuous phase viscosities as a result of the increase in the film drainage times. The increase (decrease) in the rate of coalescence for w/o (o/w) dispersions gives rise to an increase (decrease) in d_{32} resulting in a decrease (increase) in the interfacial energy. A similar increase in λ results in a decrease (increase) in the breakup probability of w/o (o/w) dispersions. This can be explained by the fact that the breakup probability is proportional to $[\exp(-\eta_d/\eta_c)]$, as shown in Eq. [4]. The resultant decrease (increase) in the breakup rate for w/o (o/w) dispersions gives rise to an increase (decrease) in d_{32}, which results in a decrease (increase) in interfacial energy. As shown in Fig. 7, which depicts the total interfacial energy per unit volume as a function of the water holdup, the effect of increasing λ therefore results in a shift of the w/o dispersion energy curve downward and that of the o/w dispersion upward. This results in an increase in the inversion holdup, which explains the observed trend in the model predictions and experimental data.

In the absence of viscosity differences, the system inverts at a holdup of 0.5 for all agitation speeds. This is in agreement with the trends predicted by McClarey and Mansoori (34), who concluded that any deviation from equivolume inversion holdups are a direct result of the viscosity difference between the two immiscible liquids alone. At the extreme ends of the viscosity ratios, the curves are observed to level off. This could be due to the fact that the exponential factor in the breakup probability reaches an asymptote at very low and very large values of the viscosity ratio. This is an important observation because the simulation should not be able to predict inversion holdups which

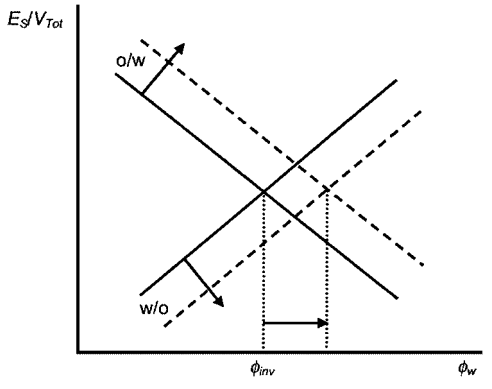

FIG. 7. Schematic illustration of the effect of increasing the water-to-oil viscosity ratio, λ, on the interfacial energy curves (E_s is the total interfacial energy, V_{Tot} the total volume, ϕ_w the water phase holdup, and ϕ_{inv} the holdup at phase inversion).

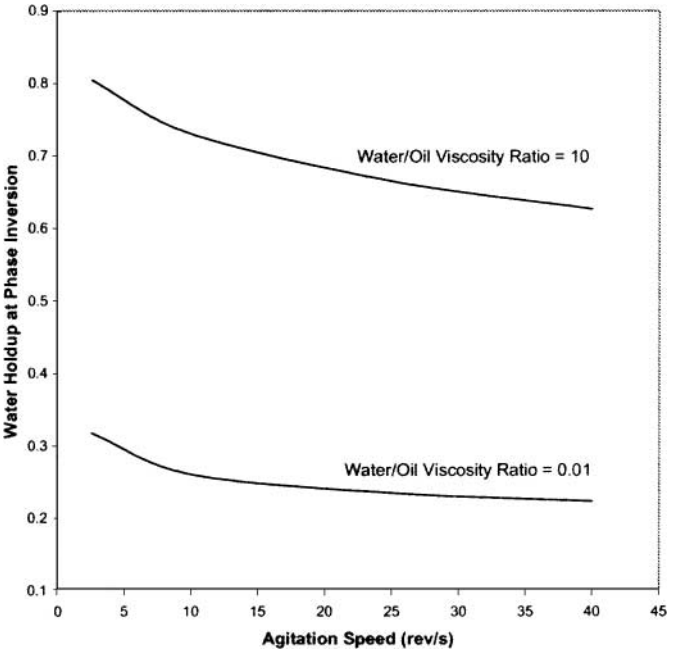

FIG. 8. Phase inversion holdup as a function of agitation speed (constant phase volume holdup).

exceed the close packing efficiency of 74.06% by a large amount as advanced theories such as the effect of the existence of secondary dispersions and the actual physical deformation of drops have not been taken into account in the present model.

The general trend indicating that the inversion holdup behaves inversely with agitation and reaches an asymptote at high agitation speeds can be seen more clearly when plotted against the agitation speed in Fig. 8. These results show qualitative agreement with the results of Quinn and Sigloh (35) and with the intermediate inversion curves of McClarey and Mansoori (34) where the organic phase holdup is held constant and inversion is introduced to the system by increasing the agitation speed from rest. An exception to these results are the observations of Vaessen (30). They note that in their experiments involving nonionic surfactant–water–oil systems, the opposite case is true; the inversion holdup is constant at low agitation speeds up to approximately 1500 r.p.m. (25 s^{-1}) but increases at high agitation speeds. This is attributed to a decrease in the coalescence probability due to shorter contact times and larger collision forces at high agitation speeds. While this agrees with the experimental observations of Shinnar (20), Park and Blair (36) have observed that coalescence increases with higher agitation speeds.

4.3. Effect of the Density Ratio on the Phase Inversion Holdup

The effect of varying liquid densities for an equal viscosity system is demonstrated in Fig. 9. It can be seen that as the water-to-oil density ratio is increased, it becomes increasingly difficult to invert the water-in-oil dispersion and hence the inversion holdup increases. While some investigators (37, 38) have generally observed increased tendencies to invert for systems in

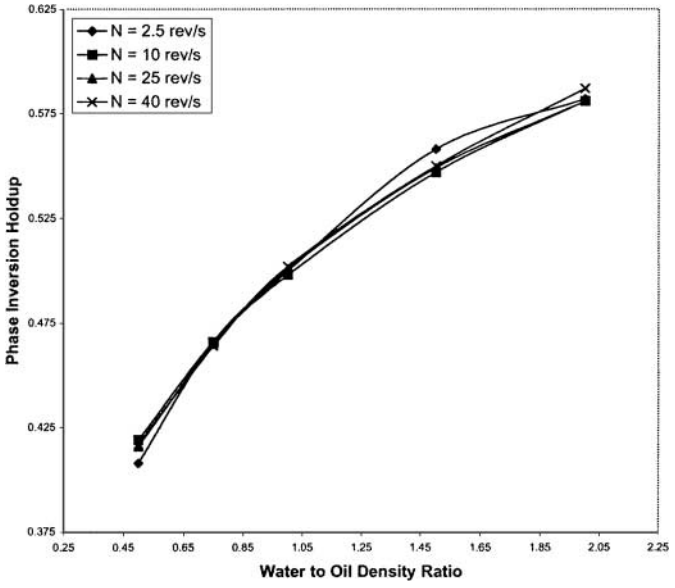

FIG. 9. Effect of water-to-oil density ratio on inversion holdup for an equal viscosity system. (Note that the lines were added to aid clear viewing of the trends rather than on a theoretical basis.)

which large density differences are evident, Chiang and Chen (39) have found that there is a lower tendency to invert in systems with large density differences if water is the dispersed phase as we have observed in our results.

The investigation into the effects of the density ratio in an equal viscosity system is not dissimilar to the study by Selker and Sleicher (31) of the effect of the kinematic viscosity ratio on phase inversion. In general, they found that the agitation speed did not have any effects on the ambivalence limits if there is adequate turbulence to prevent settling. Quinn and Sigloh (35) also noted that the inversion holdup tends toward an asymptote at high degrees of agitation. This is observed in the results shown in Fig. 9 where the effects of agitation are not evident.

4.4. Effect of Interfacial Tension on the Phase Inversion Holdup

Selker and Sleicher (31) postulated that interfacial tension is not likely to affect the inversion of a liquid–liquid dispersion because to suggest the contrary would require the implication that interfacial tension is a function of the curvature of the interface. Nevertheless, they did not substantiate their argument with extensive experimental observations. Our simulations show that interfacial tension does indeed affect inversion behavior as seen in Fig. 10 for an equidensity system. For systems in which no viscosity or density differences exist, interfacial tension does not have any effect on the phase inversion holdup; the system therefore inverts at equivolume holdup. This is in agreement with (32) who suggested that the inversion holdup is 50% in systems in which forces other than interfacial tension are absent.

For systems in which the oil phase viscosity exceeds the aqueous phase viscosity, the curves at the bottom of Fig. 10 indicate that inversion from the water-in-oil dispersion morphology to the oil-in-water dispersion morphology with increasing interfacial tension takes place at higher holdups. On the other hand, for systems in which the aqueous phase viscosity is greater than that of the organic phase, as seen by the curves at the top of Fig. 10, phase inversion occurs at lower holdups for increasing interfacial tension. The experiments of Clarke and Sawistowski (40), Norato *et al.* (41), and Dong and Tsouris (42) have shown that lowering the interfacial tension (in the range 8.9 to 39 dynes/cm) widens the gap between the ambivalence curves, indicating an

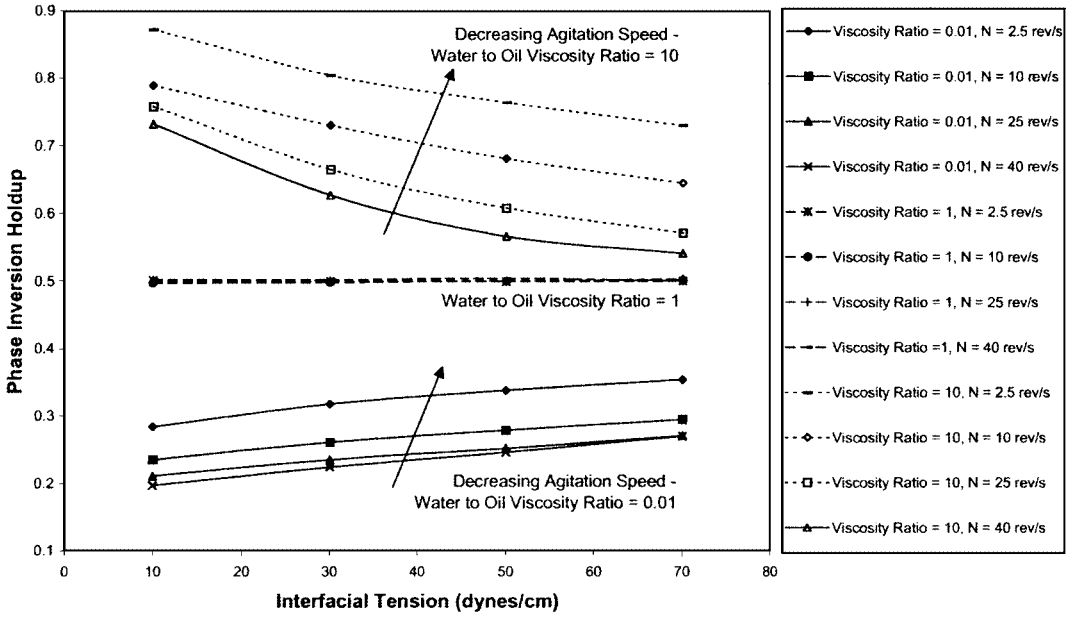

FIG. 10. Variation of the phase inversion holdup with interfacial tension for different water-to-oil viscosity ratios.

increase in the difficulty of inversion. These observations confirm the predictions of our model because (40–42) used liquids in which the aqueous phase to organic phase viscosity ratios are greater than unity. On the other hand, there is insufficient experimental evidence to verify the predictions for the case where the aqueous phase to organic phase viscosity ratios are below unity.

Norato *et al*. (41) explain their observations by suggesting that the rate of breakup increases, whereas the rate of coalescence decreases when interfacial tension is lowered, leading to higher inversion holdups. The increase in the breakup rate due to a decrease in the interfacial tension is clear. However, there are two opposing effects of interfacial tension on coalescence:

- Film drainage—Increasing the interfacial tension rigidifies the interface between the film and the drops, thereby decreasing the film drainage times, leading to an increase in the coalescence probability and hence a corresponding increase in the rate of coalescence as shown by Eq. [12].
- Drop deformation energy—An increase in the interfacial tension results in an associated increase in the energy required to deform the drop. As a result, there is a reduction in the coalescence probability and hence a suppression of the coalescence rate for a constant energy of collision between two drops. This is reflected by the expression for the rate of coalescence given by Eq. [13].

For high dispersed to continuous phase viscosity ratios, the interface between the film and the drop is rendered immobile. The time taken for the film to drain to its critical rupture thickness is therefore large. In this case, the film drainage is the limiting factor; an increase in interfacial tension is thus likely to affect film drainage, thereby causing an increase in coalescence and a consequent decrease in the phase inversion holdup. In addition, an increase in the interfacial tension results in a decrease in the interfacial area, leading to larger mean drop sizes. As a consequence, there is an enhancement in the coalescence frequency, resulting in increased rates of coalescence and subsequently lower phase inversion holdups. On the other hand, when the dispersed phase viscosity is low compared to that of the continuous phase, the interface is mobile to a certain degree. The drop deformation energy is therefore the limiting factor for the coalescence process, and therefore the coalescence rate is retarded as a result of the higher energies required to deform the drops as interfacial tension is increased. Higher phase inversion holdups are therefore observed.

5. CONCLUSIONS

We have presented a method for predicting phase inversion of concentrated liquid–liquid dispersions in agitated vessels via a Monte Carlo technique utilizing the interfacial energy minimization as the criterion for phase inversion. This work offers a number of significant advantages over previous simulation studies (6) by incorporating into the model the fundamental dependence of drop deformation, coalescence, and breakup on physical and physicochemical system parameters. Furthermore, this paper presents a framework in which drop interpenetration, an inevitable consequence of simulating concentrated dispersions of "rigid" drops, can be interpreted as drop deformation. Excessive interpenetration is penalized by introducing a penalty function, which is related to the energy of deformation of drops and the level of turbulence available to bring into effect this deformation. These features of the algorithm employed allow the investigation of phase inversion of w/o and o/w dispersions up to phase volume holdups in excess of 80% for a variety of system parameters.

The current model, however, cannot predict the presence of hysteresis effects, which often accompany phase inversion. This is because the criterion used for phase inversion, i.e., interfacial energy minimization, requires the comparison of the total interfacial energy of both dispersion morphologies to obtain a single value for the phase inversion holdup. Initiating the simulation with an o/w dispersion instead of a w/o dispersion therefore does not produce a different value for the phase inversion holdup. This limitation poses difficulties in obtaining direct validation of model predictions against experimental results. Inspections of the results of our simulations nevertheless reveal good qualitative agreement with experimental observations. For instance, salient features, which cannot be predicted a priori such as inversion at equivolume holdups in the absence of viscosity differences and the insensitivity of the phase inversion holdup to agitation speed for sufficiently large speeds, are captured by our simulations.

It is planned to further develop the current version of the algorithm to take into account complex processes such as drop charge and wall wetting effects as well as the presence of secondary dispersions. These processes may in fact play an important role in the development of hysteresis effects manifested by the presence of the ambivalence region, a key feature of phase inversion. The results of the present study, while not providing any further elucidation of the mechanism by which phase inversion occurs, nevertheless indicate that a Monte Carlo-type technique may be a useful predictive tool that can be employed to determine quantitatively the conditions under which phase inversion occurs in concentrated liquid–liquid dispersions.

APPENDIX

Determination of the Equatorial Radii for Prolate Spheres

In Section 3.5, drop interpenetration as a consequence of high-phase volume holdups was interpreted as drop deformation within the framework of the present model. The drops were assumed to deform into prolate spheroids whose centers are taken to be the centers of the originally undeformed spherical drops (Fig. 3). Since the coordinates of the centers of the drops as well as the drop radii, r_1 and r_2, are known, then the separation between the centers of the drops, L, can be found.

Given the assumption that the centers of both the original undeformed spherical drops and the resultant prolate spheroids

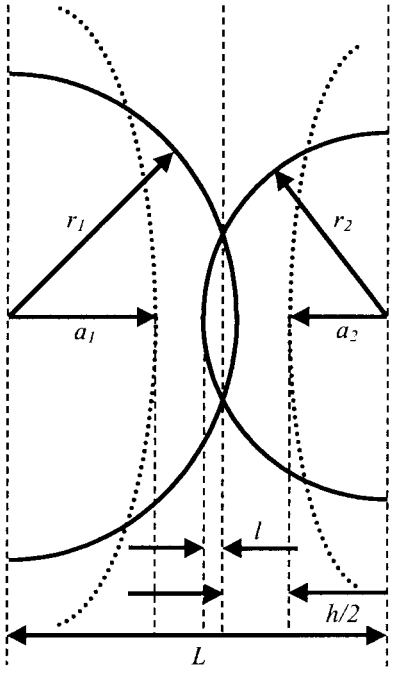

FIG. 11. Deformation of two initially spherical drops, of radii r_1 and r_2 and with separation L between their centers, to prolate spheroids with equatorial radii a_1 and a_2, and polar radii c_1 and c_2—determination of the equatorial radii. h is the thickness of the thin continuous fluid film between the deformed drops.

are the same, then it can be seen from Fig. 11 that

$$a_i = r_i - \frac{h}{2} - l_i, \qquad [28]$$

where a_i is the equatorial radius of the prolate spheroid formed from drop i with radius r_i before any deformation took place ($i = 1, 2$). h is the resulting film thickness between the two prolate spheroids, as determined by Eqs. [24] and [25] and l_i is some distance between the radial dimension of the originally undeformed spherical drop and some point along the axis at which the interpenetration between the originally undeformed spherical drops is at its maximum. To simplify the model, we assume that

$$l_1 = l_2 = l, \qquad [29]$$

where it follows that

$$l = \frac{r_1 + r_2 - L}{2}. \qquad [30]$$

Therefore, from Eqs. [28] and [30], the equatorial radius for prolate spheroid i is determined by

$$a_i = \frac{1}{2}(\pm r_1 \mp r_2 - h + L), \qquad [31]$$

where the signs on the top correspond to $i = 1$ and those on the bottom correspond to $i = 2$ respectively.

REFERENCES

1. Yeo, L. Y., Matar, O. K., Perez de Ortiz, E. S., and Hewitt, G. F., *Multiphase Sci. Tech.* **12,** 51 (2000).
2. Jiang, Y., Swart, P. J., Saxena, A., Asipauskas, M., and Glazier, J. A., *Phys. Rev. E* **59,** 5819 (1999).
3. Hsia, M. A., and Tavlarides, L. L., *Chem. Eng. J.* **20,** 225 (1980).
4. Ribeiro, L. M., Regueiras, P. F. R., Guimarães, M. M. L., Madureira, C. M. N., and Cruz-Pinto, J. J. C., *Comp. Chem. Eng.* **19,** 333 (1995).
5. Balmelli, M., and Steiner, L., *Chem. Eng. Proc.* **39,** 201 (2000).
6. Juswandi, J., M.S. Thesis. Oklahoma State University, 1995.
7. Brooks, W. B., and Richmond, H. N., *Chem. Eng. Sci.* **49,** 1843 (1994).
8. Luhning, R. W., and Sawistowski, H., *in* "Proceedings of the International Solvent Extraction Conference" (J. G. Gregory, B. Evans, and P. C. Weston, Eds.), Vol. 2, p. 873. Society of Chemical Industry, London, 1971.
9. Fakhr-Din, S. M., Ph.D. Thesis. University of Manchester, 1973.
10. Tidhar, M., Merchuk, J. C., Sembira, A. N., and Wolf, D., *Chem. Eng. Sci.* **41,** 457 (1986).
11. Metropolis, N., Rosenbluth, A. W., Rosenbluth, M. N., Teller, A. H., and Teller, E., *J. Chem. Phys.* **21,** 1087 (1953).
12. Hinze, J. O., *AIChE J.* **1,** 289 (1955).
13. Batchelor, G. K., *Proc. Cambridge Phil. Soc.* **47,** 359 (1951).
14. Bałdyga, J., and Podgórska, W., *Can. J. Chem. Eng.* **76,** 456 (1998).
15. Cutter, L. A., *AIChE J.* **12,** 35 (1966).
16. Zhou, G., and Kresta, S. M., *Chem. Eng. Sci.* **53,** 2063 (1998).
17. Coulaloglou, C. A., and Tavlarides, L. L., *Chem. Eng. Sci.* **32,** 1289 (1977).
18. Sovová, H., *Chem. Eng. Sci.* **36,** 1567 (1981).
19. Chesters, A. K., *Chem. Eng. Res., Design Trans. IChemE A* **69,** 259 (1991).
20. Shinnar, R., *J. Fluid. Mech.* **10,** 259 (1961).
21. Chen, H. T., and Middleman, S., *AIChE J.* **13,** 989 (1967).
22. Abid, S., and Chesters, A. K., *Int. J. Multiphase Flow* **20,** 613 (1994).
23. Bazhlekov, I. B., Chesters, A. K., and van de Vosse, F. N., *Int. J. Multiphase Flow* **26,** 445 (2000).
24. Tsouris, C., and Tavlarides, L. L., *AIChE J.* **40,** 395 (1994).
25. Li, D., and Liu, S., *Langmuir* **12,** 5216 (1996).
26. Liu, S., and Li, D., *Chem. Eng. Sci.* **54,** 5667 (1999).
27. Soppe, W., *Powder Tech.* **62,** 189 (1990).
28. Yeo, L. Y., Matar, O. K., Perez de Ortiz, E. S., and Hewitt, G. F., *in* "Proceedings of the International Symposium on Multi-phase Flow and Transport Phenomena" (D. M. Maron, Ed.), p. 144. Begell House, New York, 2000.
29. Lachaise, J., Mendiboure, B., Dicharry, C., Marion, G., and Salager, J. L., *Colloid Surf. A* **110,** 1 (1996).
30. Vaessen, G. E. J., Ph.D. Thesis. Eindhoven University of Technology, 1996.
31. Selker, A. H., and Sleicher, Jr., C. A., *Can. J. Chem. Eng.* **43,** 298 (1965).
32. Yeh, G. C., Haynie, Jr., F. H., and Moses, R. A., *AIChE J.* **10,** 260 (1964).
33. Arirachakaran, S., Oglesby, K. D., Malinowsky, M. S., Shoham, O., and Brill, J. P., Paper SPE 18836. Society of Petroleum Engineers, Oklahoma 1989.
34. McClarey, M. J., and Mansoori, G. A., *in* "Fundamental Aspects of Hydrometallurgical Processes" (T. W. Chapman, L. L. Tavlarides, G. L. Hubred, and R. M. Wellek, Eds.), AIChE Symposium Series, Vol. 74, No. 173, p. 134. American Institute of Chemical Engineers, New York, 1978.
35. Quinn, J. A., and Sigloh, D. B., *Can. J. Chem. Eng.* **41,** 15 (1963).
36. Park, J. Y., and Blair, L. M., *Chem. Eng. Sci.* **30,** 1057 (1975).
37. Rodger, W. A., Trice, Jr., V. G., and Rushton, J. H., *Chem. Eng. Prog.* **52,** 515 (1956).
38. Kumar, S., Kumar, R., and Gandhi, K. S., *Chem. Eng. Sci.* **46,** 2365 (1991).
39. Chiang, C. L., and Chen, C. M., *J. Chinese Inst. Chem. Eng.* **25,** 367 (1994).
40. Clarke, S. I., and Sawistowski, H., *Trans. IChemE* **56,** 50 (1978).
41. Norato, M. A., Tsouris, C., and Tavlarides, L. L., *Can. J. Chem. Eng.* **76,** 486 (1998).
42. Dong, J., and Tsouris, C., *J. Disp. Sci. Tech.* **22,** 57 (2001).